

estimate of the Wiener window. However, the typical form of such data means that good empirical parametric models are invariably available, so that accurate estimates of the Wiener window can be made. Of course, one might expect that if the models are sufficiently accurate then the deconvolution can be performed on the models themselves, thereby bypassing any consideration of the Wiener filter. In this communication it was shown that such a crossover point in model accuracy does exist, one side of which the best results are obtained with the standard Wiener filter (W_3) and the other side of which it is better to perform a straightforward deconvolution of the models themselves using, for example, the method of serial division [9].

So far, it has not been demonstrated, either theoretically or by example, that W_2 can ever perform better than both W_1 and W_3 . Indeed, experience seems to indicate that, while W_2 may certainly perform better than W_1 , under those conditions when it does then W_3 seems to perform better than either. The choice of Wiener window is thus reduced to that of W_1 (which is tantamount to using the model $\bar{y}(t)$ itself with no window at all) or W_3 (the usual form). Although it appears difficult to make specific statements about when to use either, the results of this study indicate that the availability of a good parametric model for $y(t)$ (such as the biexponential model of the above example) would allow the use of W_1 . The definition of a good model here means one whose residuals (the differences between the model and the signal being modeled) are noise-like in character. A poorer model, whose residuals would exhibit systematic deviations about zero (indicating insufficient degrees of freedom or inappropriate structure, such as the parametric but highly inappropriate polynomial model in Fig. 3) would require the use of W_3 .

In conclusion, then, it is possible to suggest the following procedure for deciding on how to use the Wiener filter in the deconvolution of tracer-type data. First, fit an appropriate parametric model to the data to be deconvolved. Next, examine the residuals between the data and the fitted model. If they are essentially noise-like in character then one should deconvolve the model itself. If the residuals have clear deterministic features (i.e., systematic deviations about zero) then one should use the model to implement the standard Wiener filter (W_3). Finally, although this study has focused on the deconvolution of biological data, its results apply equally well to any data whose deterministic part is smooth and well representable by a parametric model.

ACKNOWLEDGMENT

The helpful comments of Dr. R. Kearney and Dr. I. Hunter are gratefully acknowledged.

REFERENCES

- [1] D. M. Foster, D. G. Covell and M. Berman, "Applications of a general method for deconvolution using compartmental analysis," *Comput. Biol. Med.*, vol. 18, pp. 253-266, 1988.
- [2] J. Gamel, W. F. Rousseau, C. R. Katholi, and E. Mesel, "Pitfalls in digital computation of the impulse response of vascular beds from indicator-dilution curves," *Circ. Res.*, vol. XXXII, pp. 516-523, 1973.
- [3] N. Wiener, *Extrapolation, Interpolation and Smoothing of Stationary Time Series*. New York: Wiley, 1949.
- [4] R. N. Bracewell, "Restoration in the presence of errors," *Proc. IRE*, vol. 46, pp. 106-111, 1958.
- [5] J. W. Brault and O. R. White, "The analysis and restoration of astronomical data via the fast Fourier transform," *Astron. Astrophys.*, vol. 13, pp. 169-189, 1971.
- [6] W. H. Press, B. P. Flannery, S. A. Teukolsky, and W. T. Vetterlin, *Numerical Recipes*. London: Cambridge Univ. Press, 1986, pp. 417-419.
- [7] D. J. Cutler, "Numerical deconvolution by least squares: Use of prescribed input functions," *J. Pharm. Biopharm.*, vol. 6, pp. 227-241, 1978.
- [8] —, "Numerical deconvolution by least squares: Use of polynomials to represent the input function," *J. Pharm. Biopharm.*, vol. 6, pp. 243-263, 1978.
- [9] R. N. Bracewell, *The Fourier Transform and its Applications*, 2nd ed. New York: McGraw-Hill, 1978.
- [10] P. V. Pedersen, "Novel deconvolution method for linear pharmacokinetic systems with polyexponential impulse response," *J. Pharm. Sci.*, vol. 69, pp. 312-318, 1980.

Numerical Implementation of Sealed-End Boundary Conditions in Cable Theory

Ernst Niebur and Dagmar Niebur

Abstract—We show that a frequently used numerical implementation of von Neumann boundary conditions (zero inflowing current) in cable theory is incorrect. Correct implementations are given and it is shown that they yield results in good agreement with known analytical solutions.

INTRODUCTION

Cable theory is the standard tool for modeling voltage distributions in spatially extended neurons or other excitable cells, like cells found in cardiac tissue. The theory is based on the observation that the intracellular electrical potential varies much more along a long nerve fiber than between points inside the fiber in a plane perpendicular to the fiber axis. This facilitates greatly the mathematical analysis since the spatial dimension of the differential equations for the intracellular voltage is reduced from three to one. The advent of digital computers made the numerical solution of these equations possible in cases in which no analytical solutions have been found.

Any method of solution, analytical or numerical, must take into account the initial conditions and the boundary conditions which make the solution of the differential equations unique. We found several articles in the literature [1], [2], [5], [6], [9], [11], [13], [16] in which the boundary conditions were incorrectly implemented, which led to a wrong solution. This communication deals with the correct implementation of the boundary conditions.

Manuscript received June 10, 1991; revised August 30, 1991. The work of E. Niebur was supported by the Swiss National Science Foundation Grants No. 2000-5.295 and 8220-25941, the Air Force Office of Scientific Research, and the James S. McDonnell Foundation. It was started at the Swiss Federal Institute of Technology (EPFL), supported by EPFL, and was completed at the Jet Propulsion Laboratory, California Institute of Technology, supported by the U.S. Department of Energy through an agreement with the National Aeronautics and Space Administration.

E. Niebur is with the Institute of Theoretical Physics, University of Lausanne, CH-1015 Lausanne, Switzerland, and Computation and Neural Systems 216-76, California Institute of Technology, Pasadena, CA 91125.

D. Niebur is with the Department of Electrical Engineering, Swiss Federal Institute of Technology, CH-1015 Lausanne, Switzerland and Jet Propulsion Laboratory, California Institute of Technology, Pasadena, CA 91109.

IEEE Log Number 9103960.

CABLE THEORY AND BOUNDARY CONDITIONS

Let $V(x, t)$ be the intracellular voltage in the nerve fiber under study, t the time, and x the space coordinate along the axis of the fiber. The basic assumption of cable theory is that V obeys the following partial differential equation [17]

$$\frac{d}{4R_i} \frac{\partial^2 V(x, t)}{\partial x^2} - C_M \frac{\partial V(x, t)}{\partial t} = j_M(x, t) \quad (1)$$

where d is the diameter of the fiber, R_i the volume resistivity of the cytoplasm, C_M the transmembrane capacity per membrane area, and $j_M(x, t)$ the transmembrane current per membrane area. If the cell membrane is passive and linear, j_M is found to be

$$j_M(x, t) = g_R \cdot (V(x, t) - E_R)$$

where g_R is the transmembrane resting conductivity per membrane area, and E_R the resting potential.¹ All arguments in this communication are, however, valid when j_M depends explicitly on x and t , or when it contains nonlinear terms in V ; e.g., in the Hodgkin-Huxley model. We will assume that d , C_M , R_i , g_R , and E_R do not depend on x or t .

Equation (1) can then be written as

$$\tau \frac{\partial V(x, t)}{\partial t} = \lambda^2 \frac{\partial^2 V(x, t)}{\partial x^2} - (V(x, t) - E_R). \quad (2)$$

where λ and τ are defined by

$$\lambda^2 = \frac{d}{4R_i \cdot g_R}, \quad \tau = \frac{C_M}{g_R}.$$

In order to obtain a unique solution of (2), initial conditions and boundary conditions (BC) have to be provided. If the length of the nerve fiber under study is L , we want to solve (2) in the spatial interval $[0, L]$ and for $t > 0$. The initial conditions are determined by the choice of $V(x, t = 0)$ for all $x \in [0, L]$:

$$V(x, 0) = V_0(x), \quad x \in [0, L], \quad (3)$$

where $V_0(x)$ is a given function of x .

The longitudinal current along the fiber is given by [17]

$$I(x, t) = -\frac{\pi d^2}{4R_i} \frac{\partial V(x, t)}{\partial x}. \quad (4)$$

Often it is a good approximation to assume that no current is leaking out of the distal ends of the nerve or cardiac fiber. One then speaks of "sealed-end boundary conditions." From (4), it is clear that the BC corresponding to vanishing leakage currents at both ends are

$$\left. \frac{\partial V(x, t)}{\partial x} \right|_{x=0} = \left. \frac{\partial V(x, t)}{\partial x} \right|_{x=L} = 0 \quad \text{for all } t. \quad (5)$$

In mathematics, this is called a von Neumann boundary condition.

NUMERICAL SOLUTION BY FINITE DIFFERENCE METHODS

The numerical solution of (2) can be obtained by finite difference methods. The time is divided in steps of Δt , and the spatial interval $[0, L]$ is divided into segments by $N + 1$ equidistant points. We define $\Delta x = L/N$, and

$$V_i^n = V(i \cdot \Delta x, n \cdot \Delta t),$$

$$i \in \{0, 1, 2, \dots, N\}, \quad n = 0, 1, 2, \dots$$

¹Units are as follows: d is in [m], R_i in [Ω m], C_M in [Fm^{-2}], j_M in [Am^{-2}], g_R in [$\Omega^{-1} \text{m}^{-2}$], and V and E_R are in [V]. It follows that the units of λ and τ , which will be defined after (2), are [m] and [s], respectively.

Using the first-order approximation for the time-derivative and central differences for the spatial derivatives, (2) is written in discretized form as

$$\alpha V_{i-1}^{n+1} + \beta V_i^{n+1} + \alpha V_{i+1}^{n+1} = \gamma_i, \quad (6)$$

$$\alpha = -\mu \frac{\lambda^2}{\Delta x^2}, \quad \beta = \frac{\tau}{\Delta t} + 2\mu \frac{\lambda^2}{\Delta x^2} + \mu,$$

$$\gamma = (1 - \mu) \frac{\lambda^2}{\Delta x^2} V_{i-1}^n + \left[\frac{\tau}{\Delta t} + (\mu - 1) \left(1 + \frac{2\lambda^2}{\Delta x^2} \right) \right] V_i^n + (1 - \mu) \frac{\lambda^2}{\Delta x^2} V_{i+1}^n + E_R,$$

for all $i \in \{1, 2, \dots, N-1\}$. The boundary terms, $i = 0$ and $i = N$, will be treated separately.

In this equation, μ is a parameter which is chosen between 0 and 1. For $\mu = 0$, Euler's algorithm is obtained. In this case, (6) is an explicit expression for V_i^{n+1} as a function of V_{i-1}^n , V_i^n , and V_{i+1}^n . For $\mu = 1$, the algorithm is called "totally implicit"; for $\mu = 1/2$, it is called the "Crank-Nicholson algorithm" [4]. The Crank-Nicholson algorithm is second-order accurate in time [10], while Euler's algorithm and the totally implicit algorithm are first order.

The initial conditions, given by (3), are taken into consideration by setting $V_i^0 = V_0(i \cdot \Delta x)$ for $i \in \{0, 1, \dots, N\}$. Let us now consider the boundary condition (5), i.e., the terms with $i = 0$ and $i = N$ in (6). We found that in [1], [2], [5], [6], [9], [11], [13], [16], the sealed-end BC, given by (5) were implemented by setting

$$V_{-1}^n = V_0^n, \quad V_{N+1}^n = V_N^n \quad \text{for all } n. \quad (7)$$

This yields

$$\begin{aligned} &(\alpha + \beta) V_0^{n+1} + \alpha V_1^{n+1} \\ &= \left[\frac{\pi}{\Delta t} + (\mu - 1) \left(1 + \frac{\lambda^2}{\Delta x^2} \right) \right] V_0^n + (1 - \mu) \frac{\lambda^2}{\Delta x^2} V_1^n + E_R, \end{aligned} \quad (8)$$

$$\begin{aligned} &\alpha V_{N-1}^{n+1} + (\alpha + \beta) V_N^{n+1} \\ &= (1 - \mu) \frac{\lambda^2}{\Delta x^2} V_{N-1}^n \\ &+ \left[\frac{\tau}{\Delta t} + (\mu - 1) \left(1 + \frac{\lambda^2}{\Delta x^2} \right) \right] V_N^n + E_R. \end{aligned} \quad (9)$$

It will be shown below that (7) does *not* implement (5). We will also give formulas which must be used instead of (7).

COMPARISON OF THE NUMERICAL SOLUTION WITH THE EXACT SOLUTION

Equation (2) can be solved analytically. Using a separation Ansatz, $V(x, t) = X(x) \cdot T(t)$, and the method of variation of constants, the general solution for the sealed-end boundary conditions, (5), is found to be,

$$V(x, t) = E_R + e^{-t/\tau} \sum_{j=1}^{\infty} A_j \exp \left[-\left(\frac{\pi j \lambda}{L} \right)^2 \frac{t}{\tau} \right] \cos \left(\frac{\pi j}{L} x \right). \quad (10)$$

In this equation, the coefficients A_j are the Fourier coefficients of the initial condition. They are determined by

$$A_j = \frac{2}{L} \int_0^L [V_0(x) - E_R] \cos \left(\frac{\pi j}{L} x \right) dx. \quad (11)$$

It is instructive to consider the case when only one of these coefficients is nonzero. In Fig. 1, we have plotted the exact solution

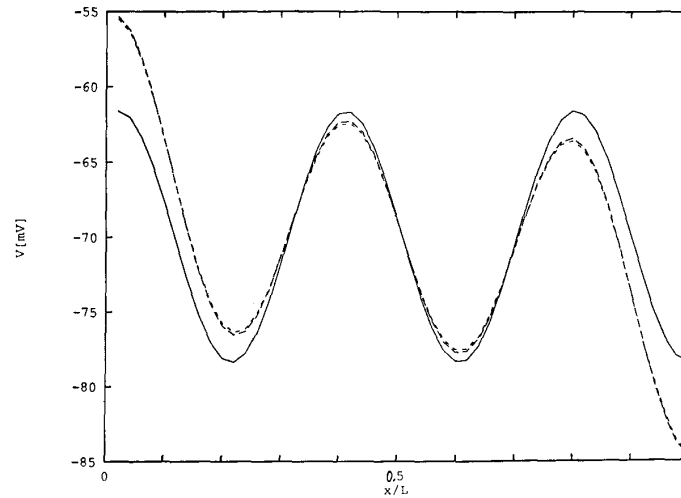


Fig. 1. Comparison of the exact and the numerical solutions of (2) representing the voltage distribution in a neural or cardiac fiber. Shown are different solutions $V(x, t = 0.01 \tau)$ of (2) versus x/L . Here, the length L of the fiber is $L = \lambda$, and the resting potential is $E_R = -70$ mV. The boundary conditions given in (7) and the initial condition given in (12) were used. The full line shows the exact solution, given by (10) and (11). The dotted line shows a numerical solution obtained using Euler's algorithm, (b) for $\mu = 0$. The dashed line shows another numerical solution, obtained using the Crank-Nicholson algorithm, (6) for $\mu = 1/2$. For both numerical solutions, $N = 50$, $\Delta x = 0.02 L$, $\Delta t = 0.67 \cdot 10^{-4} \tau$. The numerical solutions differ from the exact solution at both boundaries.

and two numerical solutions (Euler and Crank-Nicholson) for the initial condition

$$V_0(x) = E_R + 100 \text{ mV} \cos\left(\frac{5\pi}{L} x\right) \quad (12)$$

i.e., $A_5 = 100$ mV and all other A_j are zero. The BC given by (7) were used for both numerical solutions. At the boundaries, both numerical solutions differ considerably from the exact solution.

The reason for this deviation can be understood by analyzing the physical meaning of the different terms in (2). Let us treat this equation in discretized form, (6), and let us consider the boundary at $x = L$. The current flowing into this point from the region $x < L$ is proportional $(V_{N-1}^n - V_N^n)/\Delta x$, which, by (10)-(12), is easily seen to be negative for all n . On the other hand, if (7) is used as boundary condition, the current flowing towards $x > L$ is identically zero. The sum of incoming and outgoing currents is thus approximated by a negative value for all time steps. This yields the same solution of the differential equation as a boundary condition for which a current leaks out of the end of the nerve fiber at all times. The value of this "phantom" current, $I_{p,N}^n$ is easily calculated as

$$I_{p,N}^n = \frac{\pi d^2}{8R_i} \frac{V_N^n - V_{N-1}^n}{\Delta x}. \quad (13)$$

This explains the negative deviation of the numerical solution in Fig. 1 from the exact value at $x = L$. The current $I_{p,N}^n$ depends on the voltage at the boundary and it vanishes for $t \rightarrow \infty$ for the solution given in (10).

An analogous argument holds for the boundary $x = 0$, where use of the BC (7) gives rise to a "phantom" current $I_{p,1}^n$ which constantly flows into the neural process. This leads to a numerical solution for V which lies above the exact solution (see Fig. 1).

CORRECT NUMERICAL SOLUTION

A correct implementation of the sealed-end BC is obtained by expanding $V(x, t)$ in a Taylor series around the endpoints of the process under study. At $x = L$,

$$V_{N+1}^n = V_N^n + \Delta x \left. \frac{\partial V}{\partial x} \right|_{x=L} + \frac{\Delta x^2}{2} \left. \frac{\partial^2 V}{\partial x^2} \right|_{x=L} + O(\Delta x^3).$$

Replacing $\partial^2 V(x = L, t)/\partial x^2$ by $(V_{N+1}^n + V_{N-1}^n - 2V_N^n)/\Delta x^2$ and using $\partial V(x = L, t)/\partial x = 0$ for all t , we obtain $V_{N+1}^n = V_{N-1}^n + O(\Delta x^3)$. The same analysis is applied at $x = 0$ and we obtain, correct to second order in Δx ,

$$V_{-1}^n = V_1^n \text{ and } V_{N+1}^n = V_{N-1}^n \text{ for all } n. \quad (14)$$

It is a well-known result of numerical analysis that these BC are preferable to (7) because they are second order in Δx and not first order, as is (7). Use of first-order BC will eventually lead to a solution which is only first order accurate on the whole interval. Indeed, (14) has been used as an implementation of sealed-end BC previously (see, e.g., [12], [18]). However, to the best of our knowledge, it has not been noted that use of the incorrect BC not only leads to an inaccurate solution, but that it introduces systematic errors ("phantom currents"). The central point of this paper is that the phantom current [see (14)] is of first order in Δx , not of second!

A result which is correct in first and second order is obtained by using (14) as BC. The equations which replace (8) and (9) are

$$\begin{aligned} & \beta V_0^{n+1} + 2\alpha V_1^{n+1} \\ &= \left[\frac{\tau}{\Delta t} + (\mu - 1) \left(1 + \frac{2\lambda^2}{\Delta x^2} \right) \right] V_0^n \\ &+ 2(1 - \mu) \frac{\lambda^2}{\Delta x^2} V_1^n + E_R. \end{aligned} \quad (15)$$

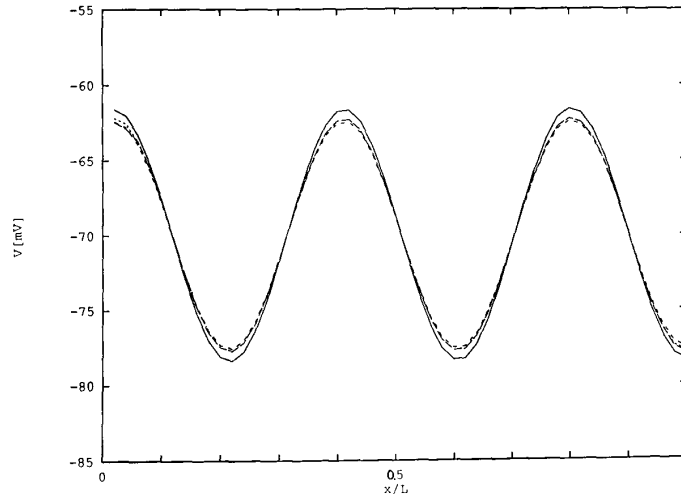


Fig. 2. Same as in Fig. 1, but the improved implementation of the boundary conditions, (15), (16) instead of (8), (9), was used for the numerical solutions. The results of the numerical calculations agree with the exact solution within the numerical error bounds.

$$\begin{aligned}
 & 2\alpha V_{N+1}^{n+1} + \beta V_N^{n+1} \\
 &= 2(1 - \mu) \frac{\lambda^2}{\Delta x^2} V_{N-1}^n \\
 &+ \left[\frac{\tau}{\Delta t} + (\mu - 1) \left(1 + \frac{2\lambda^2}{\Delta x^2} \right) \right] V_N^n + E_R. \quad (16)
 \end{aligned}$$

These BC have been used for the calculation of the numerical solutions shown in Fig. 2. They coincide with the exact solution within the numerical error bounds.

An alternative implementation of sealed-end BC has been described by Ganapathy, Clark, and Wilson [7], [8]. Instead of using central differences for the second derivative everywhere (which necessitates the introduction of a "fictitious" point at each boundary), these authors use central differences inside the integration region and forward and backward differences at the left and right boundaries, respectively. While both methods are of second-order, an obvious advantage of the forward/backward difference method is that it uses the information from two points inside the interval (e.g., V_0 and V_1), while the central difference method described above only uses one point (e.g., V_1). On the other hand, the central difference condition $V_{-1} = V_1$ reflects immediately a property of the exact solution, namely being an even function with respect to the boundary. Which method is preferable depends probably on the details of the problem to be solved.

RESULTS FOR $t \cong \tau$

Another example which shows the influence of the BC is shown in Fig. 3. It is based on one of the classical papers of the application of cable theory to nerve fibers [16] by Rall. This author simulated the excitation of a neuron by excitatory synapses by subtracting a term $g_e(x)/g_R \cdot (V(x, t) - E_e)$ from the right-hand-side of (2). (Here, e refers to "excitatory.") In this equation, $E_e > E_R$, and $g_e(x)$ is positive for those values of x , at which active synapses are present, and zero otherwise. Inhibitory synapses are simulated by subtracting a term with $E_e < E_R$ or $E_e = E_R$. This is a powerful model which recently has been generalized for simulating networks of interacting neurons [14], [15].

Sealed-end BC were used for the numerical calculations in [16]. Although the author did not state explicitly how he implemented these BC, he almost certainly used (7). We conclude this from the fact that we were able to reproduce his results perfectly well when we used this equation (compare Fig. 3, dotted lines, with Fig. 6 in [16]). On the other hand, if (14) is used, the result is different (full lines in Fig. 3). We emphasize this difference, since in our previous example (Figs. 1 and 2), we calculate the time evolution of $V(x, t)$ only over a time interval of 0.01τ , and we noted that the "phantom" current vanishes for $t \rightarrow \infty$. One might argue that the difference between the results using the correct BC, (14), and the incorrect BC, (7), is only a transient effect, which disappears rapidly. The calculation whose results are shown in Fig. 3 proves that this is not the case, and that the results depend on the implementation of the BC even at a time of the order of magnitude of τ .

EXCITATION BY INJECTION OF CURRENT

Among the papers in which the sealed-end BC are implemented by expressions equivalent to (7) is [11] by Maglaveras *et al.*; see the discussion following their (6). For other calculations, however, these authors used a boundary condition which is equivalent to our (14); see their (4). Their interpretation of this equation was, however, entirely different from ours: Maglaveras *et al.* were interested in constructing BC which make the cardiac fibers they simulate behave as if they were longer than the part which is actually simulated. This can be desirable to save computer time. Because the BC given in (14) are symmetric with respect to the boundaries (since $V_{-1}^n = V_1^n$, and $V_{N+1}^n = V_{N-1}^n$), they called these "symmetric propagation BC" and concluded that use of (14) yields a simulation of a cardiac fiber of twice the length than that of the fiber simulated explicitly and thus helps "to avoid artifacts due to impedance mismatch." Maglaveras *et al.* studied the excitation of a cardiac fiber by a current which is injected at the end of the fiber. Their calculation yielded the result that a greater current has to be injected at an end with the BC given in (14), than at an end with the BC given in (7), if the same effect (in terms of strength-duration characteristics) is to be obtained. Maglaveras *et al.* concluded that this result

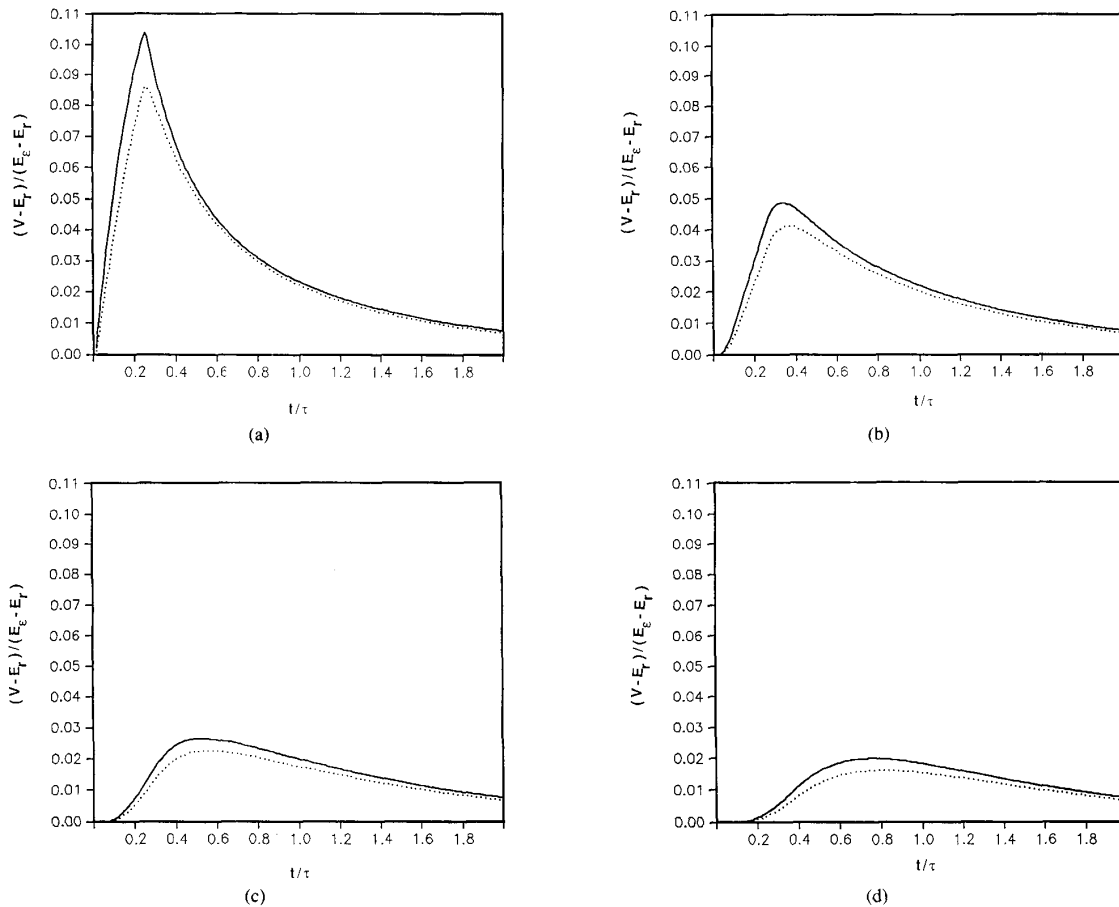


Fig. 3. (a)–(d) Simulation of a neural fiber which is postsynaptic to excitatory synapses. The fiber length $L = 2\lambda$ has been divided in ten segments ($N = 10$) for the numerical calculations. As in [16], the quantity $(V - E_r)/(E_e - E_r)$ is plotted versus time. Here, $E_r = -70$ mV, $E_e = 0$ mV, and V is the intracellular voltage in the first segment, which, in [16], was assumed to represent the soma. The synaptic excitation is assumed to take place for $0 < t < 0.25\tau$. The synaptic transmembrane conductivity in (19), g_s , is zero everywhere except in the following segments: segments 2 and 3 for 3(a), 4 and 5 for (b), 6 and 7 for (c), and 8 and 9 for (d). The synaptic interaction is assumed to be limited to these segments where it is simulated by setting $g_s = g_R$ for $0 < t < 0.25\tau$. Euler's algorithm was used in all cases and the initial conditions were always $V_0(x) = E_r$ for all x . The data shown by the dotted lines, which agree with those presented in Fig. 6(a)–(d) of [16], were calculated using the boundary conditions given in (7). The full lines show the result of the same calculation, but using the improved boundary conditions, (14). In all cases, it is clear that the results depend on the type of boundary conditions used.

corroborated their interpretation that the apparent length of the fiber is doubled.

We do not agree with this conclusion. A greater injected current is needed to achieve the same effect at an end with correctly implemented sealed-end BC than at an end with the BC given by (7), since in the latter case, the effect of the injected current is amplified by the above mentioned "phantom" current. Results obtained with this BC have thus to be considered as incorrect. The solutions Maglaveras *et al.* obtained with their "symmetric propagation BC" are valid for a sealed end. We show in the following that they can be reinterpreted for a process of double length, but that this does not lead to new results.

Let us consider a nerve fiber which has all parameters identical to the one studied above, but which extends from $x = -L$ to L , while the original fiber extended from 0 to L . If a current I is injected at $x = 0$, currents of equal magnitude $|I|/2$ flow to the right ($x > 0$) and to the left ($x < 0$). As a consequence, $\partial V/\partial x$ is non-zero for $x \neq 0$, taking the values $\partial V(-x, t)/\partial x = -\partial V(x, t)/\partial x = 4R_s I/(\pi d^2)$ [see (4)]. It follows that V has an extremum at $x =$

0 (a maximum or a minimum, depending on the sign of the injected current), thus $\partial V(x = 0, t)/\partial x = 0$ for all t . Because the same condition is met at a sealed end, injection of a current I in a cable of infinite length leads to the same solution $V(x, t)$ as injection of a current $I/2$ close to the sealed end of a half-infinite cable.² For $x < 0$, it follows from the symmetry of the problem that $V(x, t) = V(-x, t)$. Thus, the "symmetric propagation BC" yield exactly the same result as the sealed-end BC, if one takes into account that twice the current has to be injected at the midpoint of a doubled fiber than at the endpoint of the original fiber. Incidentally, (14) was already used by Cooley and Dodge [3] for the simulation of a nerve fiber which is excited by current injection at its midpoint. These authors, however, noted correctly that a pair of mirror-symmetric impulses arises at the stimulating electrode and propagate away in both directions.

²The current cannot be injected at $x = 0$ because of the sealed-end BC, but we can assume it to be injected between 0 and Δx .

ACKNOWLEDGMENT

We thank P. Erdős and C. Koch for a critical reading of the manuscript.

REFERENCES

[1] J. P. Barach and J. P. Wikswo, "Computer simulation of action potential propagation in separated nerve fibers," *Biophys. J.*, vol. 51, pp. 177-183, 1987.
 [2] J. P. Barach, "Simulation of action-potentials in a one-dimensional bidomain," *IEEE Trans. Biomed. Eng.*, vol. BME-35, pp. 340-345, May 1988.
 [3] J. W. Cooley and F. A. Dodge, "Digital computer solutions for excitation and propagation of the nerve impulse," *Biophys. J.*, vol. 6, pp. 583-599, 1966.
 [4] J. Crank and P. Nicholson, "A practical method for the numerical evaluation of partial differential equations of the heat conducting type," in *Proc. Cambridge Phil. Soc.*, vol. 43, 1947, p. 50.
 [5] N. Dimitrova, "Mathematical modeling of intra- and extracellular potentials generated by active structures with short regions of increased diameters," *Gen. Physiol. Biophys.*, vol. 7, pp. 401-412, 1988.
 [6] —, "Theoretical study of transmembrane and extracellular potentials under propagation block due to geometrical inhomogeneity," *Gen. Physiol. Biophys.*, vol. 7, pp. 581-589, 1988.
 [7] N. Ganapathy and J. W. Clark, "Extracellular currents and potentials of the active myelinated nerve fiber," *Biophys. J.*, vol. 52, pp. 749-761, 1987.
 [8] N. Ganapathy, J. W. Clark, and O. B. Wilson, "Extracellular potentials from skeletal muscle," *Math. Biosci.*, vol. 83, pp. 61-96, 1987.
 [9] R. W. Joyner, M. Westerfield, J. W. Moore, and N. Stockbridge, "A numerical method to model excitable cells," *Biophys. J.*, vol. 22, pp. 155-170, 1978.
 [10] H. B. Keller, "The numerical solution of parabolic partial differential equations," in *Mathematical Methods for Digital Computers*, A. Ralston and H. S. Wilf, Eds. New York: Wiley, 1967.
 [11] N. Maglaveras, A. V. Sahakian, and G. A. Myers, "Boundary conditions in simulations of cardiac propagating action potentials," *IEEE Trans. Biomed. Eng.*, vol. BME-35, pp. 755-758, Sept. 1988.
 [12] M. M. Mascagni, "Numerical methods for neuronal modeling," in *Methods in Neuronal Modeling*, C. Koch and I. Segev, Eds. Cambridge, MA: MIT, 1989, pp. 439-484.
 [13] J. W. Moore, F. Ramòn, and R. W. Joyner, "Axon voltage clamp simulation I: Methods and tests," *Biophys. J.*, vol. 15, pp. 11-24, 1975.
 [14] E. Niebur, "Théorie du système locomoteur et neuronal des Nématodes," Ph.D. thesis, Univ. Lausanne, Switzerland, 1988.
 [15] E. Niebur and P. Erdős, "Computer simulation of electrotonic neural networks," in *Computer Simulation in Brain Science*, R. Cotterill, Ed. UK: Cambridge Univ., 1988, pp. 148-163.
 [16] W. Rall, "Theoretical significance of dendritic trees for neuronal input-output relation," in *Neural Theory and Modelling*, R. F. Reiss, Ed. Palo Alto, CA: Stanford Univ., 1964, pp. 73-97.
 [17] W. Rall, "Core conductor theory and cable properties of neurons," in *Handbook of Physiology*, vol. 1, E. R. Kandel, Ed. Bethesda, MD: Amer. Physiol. Soc., 1977, pp. 39-98.
 [18] A. A. Sod, *Numerical Methods in Fluid Dynamics*. Cambridge, UK: Cambridge Univ., 1985.

A Bivariate Version of Andrews Plots

James A. Koziol and Werner Hacke

Abstract—A bivariate version of Andrews plots is introduced for naturally paired multivariate data. The bivariate Andrews plots are space

Manuscript received May 6, 1991; revised August 30, 1991.
 J. A. Koziol is with the Department of Molecular and Experimental Medicine, Research Institute of Scripps Clinic, La Jolla, CA 92037.
 W. Hacke is with the Neurologische Klinik, Universität Heidelberg, D-6900 Heidelberg 1, Germany.
 IEEE Log Number 9103961.

curves, and are particularly effective for revealing patterns and clusters when depicted dynamically. Projections of the bivariate Andrews plots recover the familiar univariate Andrews plots.

I. INTRODUCTION

Andrews [1] described a graphical method of obtaining a visual representation of multivariate data. The method consists of representing a p -dimensional vector $x^T = (x_1, x_2, \dots, x_p)$ (where T denotes the transpose of the $p \times 1$ column vector x) by the finite Fourier series $f_x(t) = x_1/\sqrt{2} + x_2 \sin(t) + x_3 \cos(t) + x_4 \sin(2t) + x_5 \cos(2t) + \dots$ and plotting $f_x(t)$ for a set of t -values in the range $-\pi \leq t \leq \pi$ (or, alternatively, replacing t by $2\pi t$ and using the range $0 \leq t \leq 1$). A set of p -dimensional observations will appear as a set of lines drawn on a plot, which is of use in exploratory data analysis. Andrews established a number of theoretical properties of such plots, and demonstrated their value in discerning patterns, clusters, and outliers in multivariate data sets.

For those not familiar with Andrews plots, this short example might be useful. Let the distribution of $x^T = (x_1, x_2)$ be bivariate normal, with mean vector μ_x and covariance matrix Σ_x given by

$$\mu_x = \begin{pmatrix} 0 \\ 0 \end{pmatrix}, \quad \Sigma_x = \begin{pmatrix} 1 & 0 \\ 0 & 1 \end{pmatrix},$$

respectively. Let $y^T = (y_1, y_2) = (x_1 \text{SGN}(x_1x_2), x_2)$ where $\text{SGN}(t) = +1$ if $t > 0$, -1 if $t < 0$. Then y_1 and y_2 still have unit normal marginal distributions, but they no longer are jointly bivariate normally distributed (since y_1 and y_2 are both positive or both negative, each with probability 0.5). The mean and covariance of y are given by

$$\mu_y = \begin{pmatrix} 0 \\ 0 \end{pmatrix}, \quad \Sigma_y = \begin{pmatrix} 1 & 2/\pi \\ 2/\pi & 1 \end{pmatrix},$$

respectively. A random sample of size 50 was drawn from the distribution of y , and the Andrews plots for these 50 vectors were drawn separately for y_1, y_2 positive and y_1, y_2 negative in Fig. 1(a) and (b), respectively. The patterns within each figure are consistent, and clearly distinguish the two figures.

The purpose of this note is to describe a bivariate version of Andrews plots. Given two vectors of observations $x^T = (x_1, x_2, \dots, x_p)$ and $y^T = (y_1, y_2, \dots, y_p)$ where the (x_i, y_i) , $i = 1, 2, \dots, p$ are naturally paired, form the functions

$$\begin{aligned} f_x(t) &= x_1/\sqrt{2} + x_2 \sin(t) + x_3 \cos(t) + x_4 \sin(2t) \\ &\quad + x_5 \cos(2t) + \dots \\ f_y(t) &= y_1/\sqrt{2} + y_2 \sin(t) + y_3 \cos(t) + y_4 \sin(2t) \\ &\quad + y_5 \cos(2t) + \dots \end{aligned}$$

and plot $(t, f_x(t), f_y(t))$ for a set of t -values in the range $-\pi \leq t \leq \pi$.

Note that the two-dimensional projections of the space curve

$$\begin{aligned} (t, f_x(t), f_y(t)) &\rightarrow (t, f_x(t)) \\ (t, f_x(t), f_y(t)) &\rightarrow (t, f_y(t)) \end{aligned}$$

recover the familiar Andrews plots. Many of the properties of Andrews plots can thus be immediately extended to the corresponding space curves. In addition, two other properties should be mentioned:

- 1) The volume swept out by rotating the space curve $(t, f_x(t), f_y(t))$